Research on Engineering Structures & Materials

www.jresm.org

Research Group

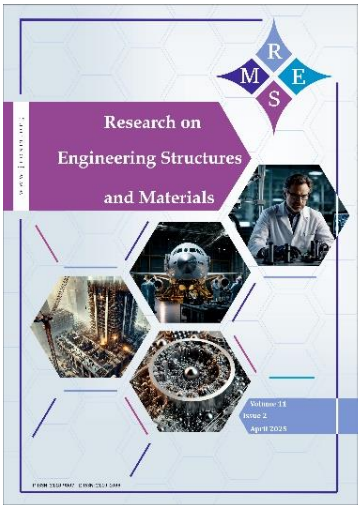

Experimental evaluation of the synergistic strengthening of concrete beams with hybrid GFRP and JFRP systems exploring bond behavior and structural performance

Idder Abdelghani, Aouadi Abdelhak, Belhocine Malika, Moulay Ali Abderrahmane, Frih Ahmed

Online Publication Date: 10 March 2026

URL: http://www.jresm.org/archive/resm2026-1426ma1221rs.html

DOI: http://dx.doi.org/10.17515/resm2026-1426ma1221rs

Journal Abbreviation: *Res. Eng. Struct. Mater.*

To cite this article

Abdelghani I, Abdelhak A, Malika B, Abderrahmane M A, Ahmed F. Experimental evaluation of the synergistic strengthening of concrete beams with hybrid GFRP and JFRP systems exploring bond behavior and structural performance. *Res. Eng. Struct. Mater.*, 2026; 12(4): 2571-2593.

Research on Engineering Structures & Materials
www.jresm.org
MIM Research Group

Research Article

Experimental evaluation of the synergistic strengthening of concrete beams with hybrid GFRP and JFRP systems exploring bond behavior and structural performance

Idder Abdelghani [*,1,a], Aouadi Abdelhak [2,b], Belhocine Malika [3,c], Moulay Ali Abderrahmane [1,d], Frih Ahmed [4,e]

[1]*Dept. of Civil Eng., Faculty of Sciences and Technology, University of Ahmed Draia Adrar, Algeria*
[2]*Dept. of Civil Eng., Faculty of Applied Sciences, University of Bouira, 10000 Bouira, Algeria*
[3]*Laboratory for Modelling of Materials and Structures in Civil Engineering (L2MSGC), Faculty of Construction Engineering, Mouloud Mammeri University of Tizi Ouzou, Tizi Ouzou 15000, Algeria*
[4]*Archipel Laboratory, Department of Civil Eng. and Hydraulics, University of Tahri Mohamed, Bechar, Algeria*

Article Info

Article History:

Received 21 Dec 2025
Accepted 04 Mar 2026

Keywords:

Testing;
Four point bending;
Sustainable concrete;
Hybrid fiber-reinforced;
Flexural strengthening;
structural rehabilitation;
Glass and jute composites

Abstract

This study explores the structural behavior and load transfer characteristics of reinforced concrete (RC) beams externally retrofitted with hybrid fiber reinforced polymer (FRP) systems combining synthetic glass fibers (GFRP) and natural jute fibers (JFRP). Fourteen full-scale RC beams were tested under four-point bending to examine how different fiber types and strengthening schemes influence both strength and deformation capacity. To monitor precise structural response, the experimental setup utilized a spreader beam for symmetrical loading and LVDTs positioned at mid-span and supports to account for settlement. While existing research often focuses on mono-material reinforcement, this work provides a new contribution by conducting a comprehensive experimental evaluation of strategic fiber positioning on full-scale specimens. The experimental results demonstrate that different configurations yield distinct performance benefits: the JFRP U-wrap configuration (JBJS) achieved a 38% increase in ultimate strength with proper anchorage, while the GFRP U-wrap reached a 44% gain. A primary novelty of this investigation is the identification of the JBGS hybrid configuration (jute along the soffit and glass on the sides) as the most balanced and resilient system tested. Despite the higher material ductility of GFRP, this specific hybrid arrangement achieved a 28% strength gain and a 71% increase in ductility index, suggesting effective stress redistribution across the reinforcement layers. Failure observations extracted from detailed crack analysis point to more gradual crack development and improved load retention in hybrid systems. These findings offer insight into performance-driven design for sustainable structural rehabilitation by demonstrating how fiber synergy can be strategically optimized to balance mechanical efficiency and eco-efficiency.

1. Introduction

Reinforced concrete (RC) remains the most widely used construction material in civil infrastructure [1-4], including bridge decks [5, 6], roadway support systems [7], and structural slabs [4, 8-11]. However, RC members are susceptible to degradation under flexural fatigue, cracking, corrosion of internal reinforcement, and environmental exposure over time [12-14].

*Corresponding author: abdelghani.idder@univ-adrar.edu.dz
[a]orcid.org/0000-0003-2795-2178; [b]orcid.org/0000-0002-5360-9990; [c]orcid.org/0009-0009-0829-8773; [d]orcid.org/0009-0008-5837-9451; [e]orcid.org/0009-0009-4515-500X
DOI: http://dx.doi.org/10.17515/resm2026-1426ma1221rs

These deteriorations compromise serviceability and safety, prompting the need for reliable strengthening and rehabilitation techniques [15-21]. The urgency of such interventions is further emphasized by the global need for seismic retrofitting, which is essential to enhance the resistivity and overall lifespan of critical elements like beam-column joints [22].

Fiber-reinforced polymer (FRP) composites have emerged as effective materials for retrofitting RC elements due to their high strength-to-weight ratio [23], corrosion resistance, and ease of application [24-32]. The increasing use of these composites is justified by their superior stiffness and favorable response under static, free vibration, and buckling conditions compared to traditional metallic materials [33]. Externally bonded FRP systems, particularly those based on glass or carbon fibers, have shown considerable success in restoring structural capacity [34-38]. However, conventional FRP systems often exhibit brittle failure modes and are associated with high production costs and environmental burdens [39-41]. These limitations have led researchers to explore the integration of natural fibers as sustainable alternatives or supplements in structural strengthening applications [42-45]. One notable example of such innovation is the investigation into using bamboo as a substitute for structural steel, which has shown promise in low-cost housing due to its appreciable tensile resistance [46]. Among natural fibers, jute has attracted interest due to its low cost, biodegradability, and acceptable tensile performance [47-52]. Nevertheless, the mechanical properties of jute are inferior to those of synthetic fibers, limiting its application in high-performance strengthening unless appropriately combined [53-57]. Recent studies have proposed hybrid systems, combining synthetic and natural fibers, to exploit their complementary properties [58-62]. Such systems aim to harness the stiffness and strength of synthetic FRPs alongside the ductility and energy absorption capacity of natural fibers, offering improved failure behavior and sustainability [63-67].

Despite the growing interest in composite materials and sustainable alternatives [68, 69], a significant research gap remains regarding the practical application of hybrid systems for the flexural strengthening of full scale reinforced concrete beams. Most existing studies are limited to theoretical reviews or experiments conducted at the material scale using small coupons which do not accurately capture the complex bond mechanics and load distribution found in real structural elements. Furthermore, while the general benefits of individual synthetic or natural fibers are well documented, there is a critical lack of evidence concerning how their strategic positioning influences structural synergy. The specific question of how to arrange high stiffness glass fibers alongside high ductility jute fibers to prevent premature debonding while maximizing both strength and deformation has not been sufficiently explored. This research addresses these deficiencies by providing a comprehensive experimental evaluation of various hybrid wrapping configurations. By investigating the interaction between fiber placement and structural performance in fourteen full scale specimens, this study establishes a clearer understanding of how to optimize hybrid reinforcements for safer and more efficient structural rehabilitation.

The beams were divided into three main categories. The first included single-material systems, where GFRP or JFRP sheets were bonded using the wet lay-up technique to either the bottom face (GB and JB) or both the bottom and side faces in a U-wrap configuration (GBGS and JBJS). The second category consisted of hybrid systems: JBGS (jute at the bottom, glass on the sides) and GBJS (glass at the bottom, jute on the sides). The final category included an unstrengthened control group (CB). All FRP fabrics were applied using an epoxy resin and arranged in a single layer per face, with particular attention given to fabric alignment and bond quality to ensure uniform load transfer. This experimental matrix was carefully designed to isolate and compare the effects of fiber type (natural vs. synthetic), reinforcement layout (bottom-only vs. U-wrap), and fiber positioning (glass vs. jute in critical tension or shear zones) on key structural parameters including strength, stiffness, ductility, and failure mode. By doing so, the study provides direct insight into how strategic fiber selection and placement can influence the mechanical behavior of strengthened RC elements under flexural loading.

The study aims to evaluate each configuration in terms of its contribution to load capacity, ductility, stiffness, and failure mechanism, thereby addressing key uncertainties in hybrid FRP retrofitting performance. In particular, it explores whether the combination of GFRP's high tensile strength and

JFRP's ecological and damping properties can produce a pseudo-ductile response, mitigating sudden brittle failure through a more progressive damage mechanism while maintaining mechanical efficiency. while maintaining mechanical efficiency. The findings provide experimental evidence to support design-oriented applications of hybrid FRP systems and demonstrate how fiber placement can be strategically optimized to balance performance and sustainability. This work contributes to advancing the development of eco-efficient, structurally reliable retrofitting methods for RC members in civil infrastructure, including pavements, bridge decks, and structural slabs.

2. Materials

The materials used in this study were selected to replicate realistic construction and retrofitting conditions while enabling a comparative evaluation of synthetic, natural, and hybrid fiber-reinforced polymer systems. This section describes the properties of the concrete matrix, epoxy adhesive, internal steel reinforcement, and externally bonded FRP composites employed in the fabrication and strengthening of the RC beam specimens.

Table 1. Concrete mix composition and design parameters per cubic meter, optimized for structural beam casting and flexural testing

Category	Material	Quantity	Remarks
Binder	Portland Cement (CEM I 42.5 R)	350 kg	High early strength, good durability
Fine Aggregates	Natural Sand (0/3 mm)	648 kg	Clean, well-graded
Coarse Aggregates	Boussaada Sand Crushed Gravel (8/15 mm) Crushed Gravel (15/25 mm)	97 kg 710 kg 400 kg	Local source, filler optimization Structural-grade angular aggregate Enhanced packing and strength
Water	Potable Water	190 L	W/C ratio of 0.54
Mix Proportions	Water-to-Cement Ratio	0.54	Targeting balanced strength/workability
Performance Targets	Aggregate-to-Cement Ratio	5.3	Moderately lean mix
	Total Aggregate Content	1855 kg	Consistent with normal-weight concrete
	Target Slump	~90 mm	Suitable for beam casting
	Design Compressive Strength	25 MPa @ 28 days	Confirmed via cube testing
	Admixtures	None	Mix achieved target without additives

2.1. Concrete

The concrete used in all beam specimens was designed to achieve a target compressive strength of approximately 25 MPa after 28 days of water curing. The mix consisted of CEM I 42.5 R Portland cement, fine aggregates (natural 0/3 mm sand and Boussaada sand), two grades of crushed gravel (8/15 mm and 15/25 mm), and potable water. A water-to-cement ratio of 0.5 was maintained to ensure sufficient workability and strength development. Mixing was carried out in a rotary drum mixer until a uniform consistency was achieved. After casting, the beams were demolded after 24 hours and cured in water at ambient temperature for 28 days. The detailed proportions of the mix components per cubic meter are provided in Table 1.

In addition to mix proportions, the water-cement ratio and fresh concrete density were determined and are presented in Table 2. The measured water-cement ratio was 0.54, slightly above the theoretical design value due to adjustments made for workability during casting. The average density of the concrete was 2390 kg/m^3, which is consistent with standard values for normal-weight structural concrete. This parameter is particularly important in the present study, as it directly influences the dead weight of the beams and the internal stress distribution under flexural loading. Accurate density values also ensure consistency when comparing load-deflection behavior across beams, especially in cases where strengthening systems alter stiffness and ductility characteristics.

Table 2. Physical and strength-related properties of fresh and hardened concrete used for casting full-scale RC beam specimens

Property	Value	Remarks
Water–Cement Ratio (w/c)	0.54	Balanced for strength and workability
Fresh Density	2390 kg/m^3	Consistent with normal-weight concrete
Hardened Density (28 days)	~2400 kg/m^3	Slight increase due to moisture loss
28-Day Compressive Strength	25 MPa	Based on cube/cylinder testing
Concrete Type	Normal-weight	No lightweight or heavyweight aggregates used
Air Content	Not measured	Estimated under 2% due to compacting process
Slump (Workability)	~90 mm	Verified during specimen casting

The dimensions and reinforcement of the beam specimens were determined based on the design principles of Eurocode 2 [70]. The specimens were specifically engineered as under-reinforced sections to ensure a ductile flexural failure mode, characterized by the yielding of the longitudinal steel reinforcement 14 mm prior to concrete crushing. To prevent premature diagonal tension failure, the stirrup spacing was calculated to provide a shear capacity significantly higher than the expected flexural capacity, ensuring that the effectiveness of the hybrid FRP strengthening could be fully evaluated in bending.

2.2. Epoxy Resin

A two-component epoxy adhesive system, NOVA MASTICOLLE, was used to bond the fiber-reinforced polymer (FRP) sheets to the concrete surfaces. This adhesive, widely employed in structural applications, offers high bond strength, compatibility with various fiber types, and ease of application using the wet lay-up method. The system, illustrated in Fig. 1, consists of a base resin (component A) and a hardener (component B), which were mixed in a weight ratio of 2:1 as recommended by the manufacturer.

Fig. 1. Two-component NOVA MASTICOLLE epoxy adhesive system used for bonding FRP sheets: Component A (resin) and Component B (hardener)

The two components were manually blended using mechanical stirring until a uniform, bubble-free mixture was achieved. The epoxy was applied to both the concrete substrate and the fiber fabric using brushes and rollers to ensure full impregnation and contact. The product exhibits a tensile strength of approximately 30 MPa and a modulus of elasticity of 3.2 GPa, making it suitable for load transfer in externally bonded reinforcement systems. Its low shrinkage, strong adhesion, and sufficient working time under ambient conditions contributed to consistent and reliable composite bonding across all specimens. The role of NOVA MASTICOLLE was essential in enabling effective stress transfer between the concrete beams and the FRP reinforcements, regardless of fiber type or configuration.

2.3. Steel Reinforcement

All beams were reinforced internally using steel bars arranged in a conventional flexural configuration. The reinforcement layout consisted of two 14 mm diameter high-adherence steel bars placed in the tension zone (bottom), two 8 mm diameter mild steel bars in the compression zone (top), and 6 mm diameter closed stirrups spaced at 100 mm along the length of the beam for shear reinforcement.

Table 3. Mechanical properties and functional roles of high-adherence and mild steel reinforcement used in RC beam specimens.

Steel Type	High-Adherence Steel	Mild Steel
Application in Beam	Bottom longitudinal bars	Top longitudinal + stirrups
Bar Diameter (mm)	14	8 (top) / 6 (stirrups)
Yield Strength (MPa)	500	235
Ultimate Strength (MPa)	550	410
Elongation (%)	12	25
Young's Modulus (MPa)	210	210
Poisson's Ratio	0.30	0.30
Remarks	Primary tensile reinforcement	Used for compression and shear

Two types of steel were used: high-adherence steel for the main tension reinforcement, and mild steel for compression and stirrup reinforcement. Mechanical properties of both steel types were obtained from uniaxial tensile tests conducted on representative samples. The high-adherence steel exhibited a yield strength of 500 MPa, an ultimate strength of 550 MPa, and an elongation capacity of 12%. The mild steel showed a lower yield strength of 235 MPa, an ultimate strength of 410 MPa, and greater ductility, with a 25% elongation capacity. Both steel types had a Young's modulus of 210,000 MPa and a Poisson's ratio of 0.3. These properties are summarized in Table 3.

The mechanical behavior of the internal steel reinforcement and the externally bonded FRP sheets was verified through uniaxial tensile testing. Fig. 2 illustrates the stress-strain relationships for these materials, highlighting the distinct yield plateau of the steel bars and the linear-elastic failure modes of the GFRP and JFRP composites.

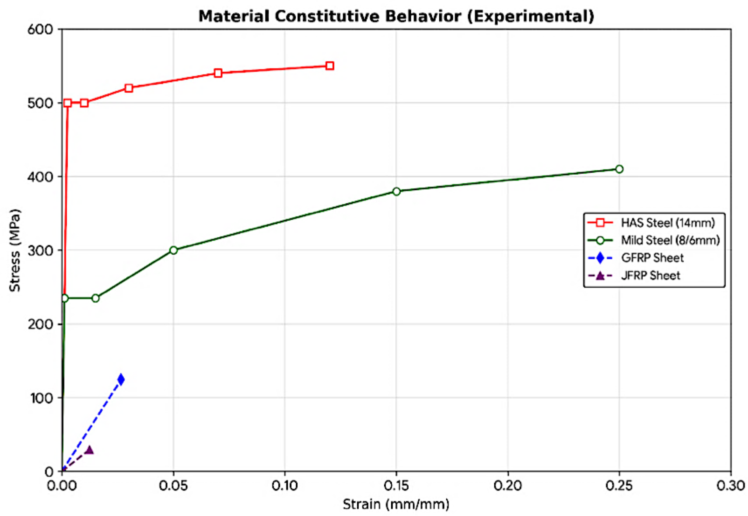

Fig. 2. Tensile stress–strain behavior of internal steel reinforcement (High-Adherence and Mild steel) and external FRP composites (GFRP and JFRP)

2.4. FRP Systems

Three externally bonded fiber-reinforced polymer (FRP) systems were employed in this study: glass fiber-reinforced polymer (GFRP), jute fiber-reinforced polymer (JFRP), and hybrid GFRP–JFRP systems. All fabrics were applied using the wet lay-up technique with NOVA MASTICOLLE epoxy resin, following surface preparation and primer application. The fibers were installed in single layers with their principal direction aligned along the longitudinal axis of the beams to ensure full contribution in flexural loading.

The GFRP sheets were unidirectional, with a nominal areal density of 850 g/m^2. They offered high tensile strength and stiffness, with a tensile strength of approximately 3200 MPa, an elastic modulus of 73 GPa, and an ultimate strain of 4.4%. The JFRP sheets, made from natural jute fibers, had lower strength but higher deformability, with a tensile strength of 250 MPa, an elastic modulus of 10 GPa, and an ultimate strain of 2.5%. The choice of jute was motivated by its environmental benefits, cost-effectiveness, and compatibility with sustainable construction strategies.

Hybrid configurations were developed by combining GFRP and JFRP sheets in specific geometric arrangements. In the JBGS configuration, jute fibers were bonded to the bottom face (tension zone) of the beam, while glass fibers were applied along the side faces to provide shear confinement. In the GBJS configuration, the positions were reversed, with GFRP at the bottom and JFRP on the sides. This hybridization aimed to exploit the stiffness and strength of synthetic fibers while benefiting from the energy absorption and ductility of natural fibers.

Table 4. Mechanical characteristics of jute and glass FRP composites prepared by wet lay-up technique, used for externally bonded reinforcement.

FRP Type	Jute FRP (JFRP)	Glass FRP (GFRP)
Elastic Modulus (GPa)	2.79	5.85
Tensile Strength (MPa)	28.54	108.96
Ultimate Stress (MPa)	29.60	124.50
Thickness (mm)	2.25	1.64
Ultimate Strain (%)	1.24	2.66

All fabrics were cut to the required dimensions and applied after saturating the surface with resin. Care was taken to ensure uniform pressure during bonding, avoid air entrapment, and maintain continuity between the fibers and the concrete substrate. The mechanical properties of both fiber types are presented in Table 4.

3. Apparatus and Operational Procedures

This section presents the experimental procedures used to investigate the flexural behaviour of RC beams strengthened with GFRP, JFRP, and hybrid FRP systems. The process included specimen preparation, application of external strengthening systems, and structural testing under four-point bending to evaluate load-bearing capacity, deformation behaviour, and failure characteristics.

The experimental program was conducted in several sequential phases to evaluate the effectiveness of the proposed hybrid strengthening systems. The overall methodology, encompassing material characterization, specimen fabrication, strengthening strategies, and structural testing, is summarized in the flowchart presented in Fig. 3.

3.1. Key Experimental Assumptions

To ensure the reliability of the comparative analysis between the fourteen specimens, the following experimental assumptions and controls were maintained:

- Batch Homogeneity: The concrete properties and internal steel reinforcement characteristics are assumed to be uniform across all specimens, as they were sourced from the same respective batches and subjected to identical curing conditions.

- Bond Consistency: The mechanical surface preparation (grinding) is assumed to have provided a standardized roughness, ensuring that variations in bond behavior are attributable to the fiber configuration rather than surface inequality.
- Application Uniformity: It is assumed that the manual wet lay-up process achieved full resin impregnation and a consistent adhesive thickness across all strengthened beams.
- Loading Symmetry: The four-point bending setup assumes perfectly symmetrical load application and leveled supports, maintaining a constant moment zone in the middle third of the span.
- Environmental Stability: Laboratory conditions were kept stable during the curing and testing phases to ensure that the mechanical response of the natural jute fibers was not influenced by significant humidity or temperature fluctuations.

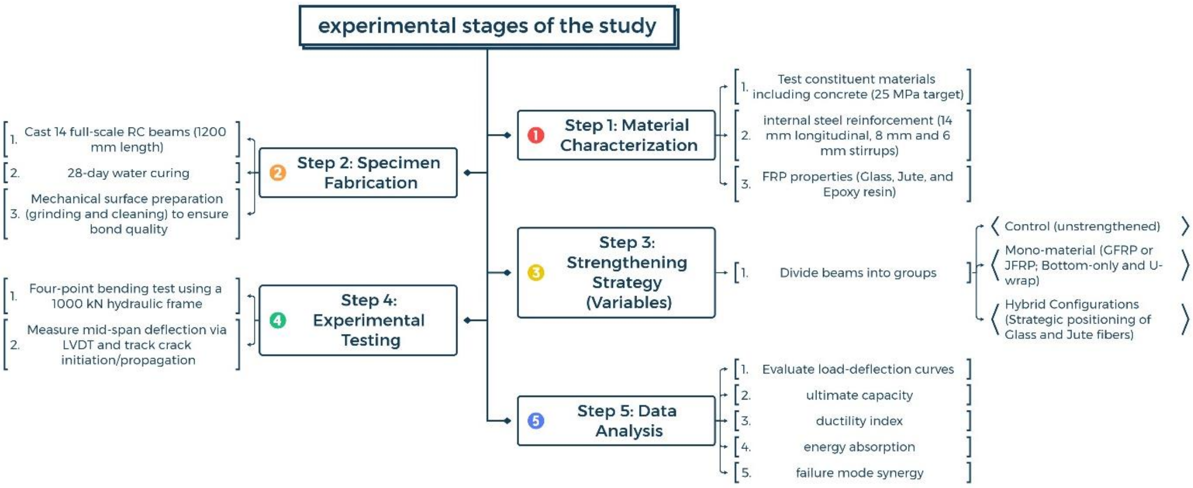

Fig. 3. Flowchart illustrating the experimental stages of the study, from material characterization to the evaluation of hybrid strengthening efficiency

3.2. Specimen Preparation

A total of fourteen full-scale RC beams were fabricated using identical formwork and reinforcement detailing. Each beam measured 600 mm in length, with a cross-section of 150 mm × 100 mm. The longitudinal reinforcement consisted of two 14 mm diameter high-adherence steel bars placed at the bottom (tension zone) and two 8 mm diameter mild steel bars placed at the top (compression zone). Transverse shear reinforcement was provided by 6 mm diameter closed stirrups spaced at 100 mm along the span. After casting, the beams were demolded after 24 hours and cured in water for 28 days.

Following curing, the concrete surfaces of all beams designated for strengthening were mechanically ground to remove surface laitance and expose the aggregate structure. Compressed air was used to clean dust and debris. This surface preparation was essential to ensure optimal bond conditions for the externally bonded FRP sheets. During specimen preparation, specific measures were implemented to ensure the reliability of the FRP-concrete bond:

- Bond Integrity: To eliminate air voids and ensure full resin impregnation, a ribbed roller was used during the wet lay-up, applying constant pressure to prevent premature debonding.
- Moisture Control: Given the hydrophilic nature of jute fibers, the JFRP sheets were pre-dried and stored in a low-humidity environment to prevent moisture from compromising the epoxy bond.
- Surface Consistency: Hand-held diamond-cup grinding was utilized to achieve a uniform ICRI CSP-3 roughness profile across all 14 beams, minimizing variability in bond performance.
- Overlap Management: In hybrid layouts (GBJS/JBGS), localized thickness at fiber intersections was mitigated by a graduated resin application to maintain a consistent cross-sectional profile.

Table 5. Experimental groups and external FRP strengthening configurations for RC beam specimens

Group	Bottom Reinforcement	Side Reinforcement	FRP Strengthening Configurations	Specimen Code	Description
0	None	None		CB	Control beam (no external reinforcement)
1	GFRP	None		GB	GFRP applied to bottom face only
2	JFRP	None	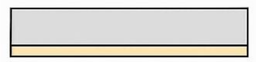	JB	JFRP applied to bottom face only
3	GFRP	GFRP		GBGS	GFRP applied to bottom and both side faces (U-wrap)
4	JFRP	JFRP	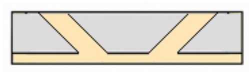	JBJS	JFRP applied to bottom and both side faces (U-wrap)
5	GFRP	JFRP	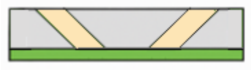	GBJS	GFRP bottom + JFRP sides (hybrid configuration)
6	JFRP	GFRP	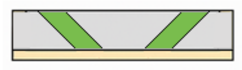	JBGS	JFRP bottom + GFRP sides (hybrid configuration)

While the experimental program was limited to two specimens per configuration (n=2) due to laboratory resource constraints, the high degree of consistency and low variability observed between the paired results justify the reliability of the reported trends. These findings provide a primary evaluation of the proposed hybrid systems, though larger sample sizes in future studies will further validate the statistical dispersion of these performance enhancements.

3.3. Strengthening Schemes and Specimen Grouping

The fourteen beam specimens were divided into seven groups based on the type and location of externally bonded reinforcement. Each group consisted of two identical beams. The experimental matrix was designed to assess the influence of fiber type (GFRP or JFRP), fiber position (bottom-only or U-wrap), and hybrid configurations (mixed fiber types) on flexural behavior. A summary of the reinforcement configurations and corresponding specimen codes is provided in Table 5.

The control group (CB) had no external reinforcement. Groups GB and JB were strengthened only at the bottom face with GFRP and JFRP, respectively. Groups GBGS and JBJS were fully wrapped in a U-shaped configuration (bottom and both side faces) using the same fiber type. The hybrid systems included JBGS, with jute at the bottom and glass on the sides, and GBJS, with the reverse arrangement. All strengthening was performed using the wet lay-up method.

The geometric dimensions, internal steel reinforcement, and experimental configuration of the beam specimens are detailed in Fig. 4. All beams shared a total length of 600 mm and a rectangular cross-section of 150 mm × 100 mm, with consistent internal steel detailing across all groups. To ensure precise data acquisition, the four-point bending setup featured a loading head connected to a spreader beam for uniform load distribution. As shown in the schematic, LVDTs were strategically positioned at the mid-span to capture maximum deflection and at the supports to monitor and account for any potential settlement during the testing process.

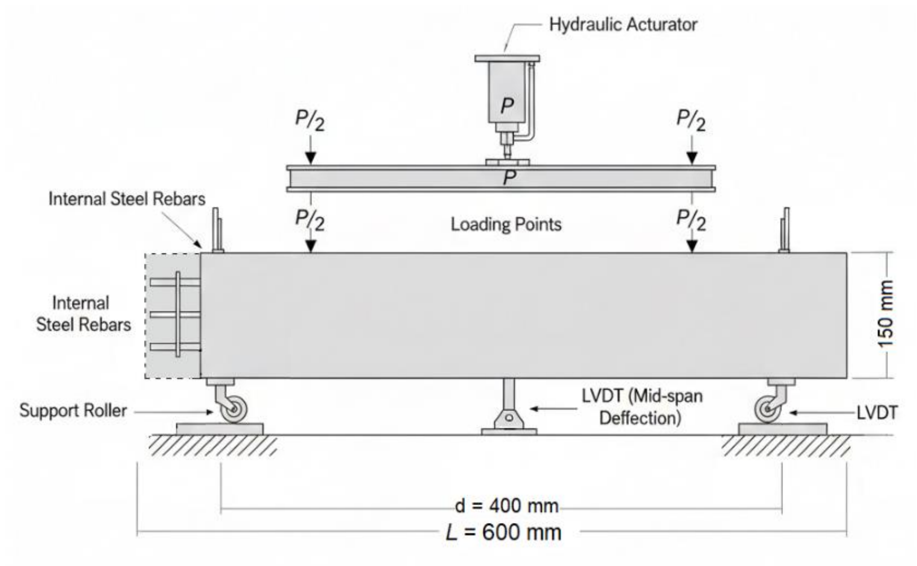

Fig. 4. Experimental test setup for a 600 mm unstrengthened RC beam under four-point loading, showing the internal reinforcement (T14 and T8 bars), stirrups (R6), and the LVDT positioning at critical measurement points

3.4. Test Setup and Instrumentation

All beams were tested under four-point bending using a hydraulic loading frame with a maximum capacity of 1000 kN. Each specimen was simply supported over a clear span of 1000 mm, with two concentrated point loads applied symmetrically at one-third points along the span, creating a constant moment region in the middle third (300 mm). This configuration is widely adopted in flexural testing to isolate bending effects and allow comparison of stiffness, strength, and ductility parameters.

Roller supports were used at both ends to allow horizontal movement and rotation, reducing constraint effects. The applied load was transmitted through a spreader beam connected to the actuator, ensuring uniform force distribution at both loading points. Loading was applied in displacement control mode at a constant rate of 2 mm/min until failure.

Fig. 5. Application of FRP strengthening systems and layout of tested configurations: bottom-only, U-wrap, and hybrid reinforcement schemes

Instrumentation was implemented to monitor both the global and localized behavior of the beams throughout testing. The applied load was measured in real time using a calibrated load cell integrated into the hydraulic actuator, with continuous data acquisition ensuring high accuracy. Mid-span deflection was recorded using a Linear Variable Differential Transformer (LVDT) positioned vertically at the center of the span. This sensor was connected to a digital acquisition system to track displacement throughout the loading process.

In addition to quantitative data, qualitative observations were also conducted. A crack monitoring system was implemented by marking the beam surfaces at regular 50 mm intervals, allowing for accurate tracking of crack formation and propagation. Crack initiation, development, and final failure modes were recorded using visual inspection and high-resolution photographic documentation. These procedures provided a comprehensive assessment of structural behavior under flexural loading and allowed for precise correlation between strengthening configuration and failure mechanism. The external appearance of the strengthened beams, showing the applied FRP systems across different configurations (bottom-only, U-wrap, and hybrid), is illustrated in Fig. 5.

4. Results and Discussion

This section presents and interprets the experimental results obtained from the four-point bending tests conducted on fourteen RC beam specimens. The beams were strengthened using various externally bonded FRP configurations GFRP, JFRP, and hybrid GFRP–JFRP systems. The analysis is organized into six subsections covering failure mechanisms, load–deflection behavior, strength performance, deformability, ductility, and the overall contribution of each configuration to structural performance.

4.1. Failure Modes

For the mechanical tests of the concrete specimens, Table 6 shows the measured properties after 28 days of curing. The compressive strength reached 36.6 MPa, determined through standard testing as illustrated in Fig. 6(a), which confirms the adequate load-bearing capacity of the mix. The tensile strength was found to be 2.79 MPa, obtained using the indirect splitting method as shown in Fig. 6(b), reflecting the brittle behavior typically associated with cementitious composites.

While the concrete mix was initially proportioned for a target compressive strength of 25 MPa, experimental testing at 28 days revealed a mean compressive strength of 36.6 MPa. This increase is attributed to the high quality of local aggregates and optimal laboratory curing conditions, which promoted a more extensive hydration process than initially anticipated. Consequently, to maintain analytical rigor, the measured value of 36.6 MPa was adopted for all subsequent theoretical calculations, flexural capacity predictions, and comparative performance analyses throughout this study. The average specimen weight was 15.47 kg, which was recorded to monitor density and ensure consistency across batches.

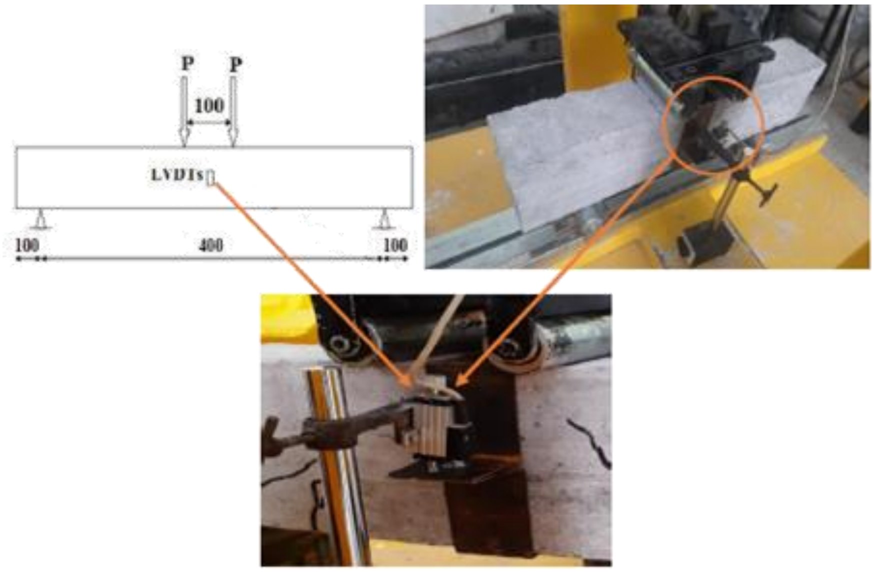

Fig. 6. Experimental test setups for concrete specimens: (a) compression testing showing the applied loading mechanism, and (b) indirect splitting tensile test used to determine the tensile strength of concrete

Failure patterns observed during testing varied significantly across the different strengthening configurations and are summarized in Table 7. The control beam (CB) failed in a typical flexural mode, with pronounced mid-span cracking followed by concrete crushing in the compression zone.

Table 6. Measured mechanical properties of 28-day cured concrete specimens.

Property	Value	Remarks
Compressive Strength ($Fc_{(28)}$)	36.6 MPa	Determined via standard cube testing
Tensile Strength ($Ft_{(28)}$)	2.79 MPa	Estimated using indirect (splitting) method
Average Specimen Weight	15.47 kg	Prism/cube weight used for density tracking

Beams strengthened with GFRP only (GB and GBGS) primarily failed due to delamination or debonding of the fiber sheet, occasionally accompanied by concrete crushing near the loading points. The brittle nature of the glass fibers contributed to sudden load drops after peak strength.

Table 7. Observed failure modes of reinforced concrete beams under four-point bending for different FRP strengthening configurations

Beam code	RC Beam concrete	Failure mode
CB	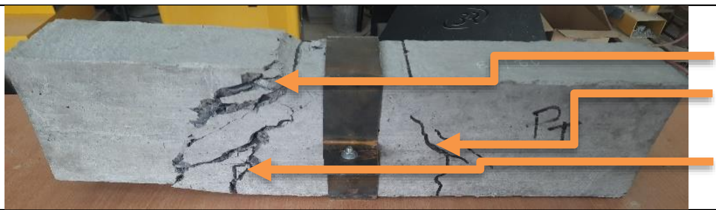	1- Crashing of concrete 2- Propagation of the shear cracks 3- Shear cracks
JB	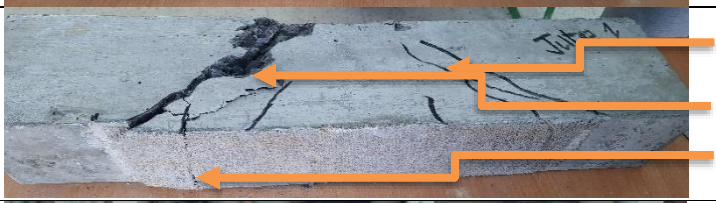	1- Propagation of the shear cracks 2- Shear cracks 3- Fracture of JFRP bands and crashing of concrete
GB	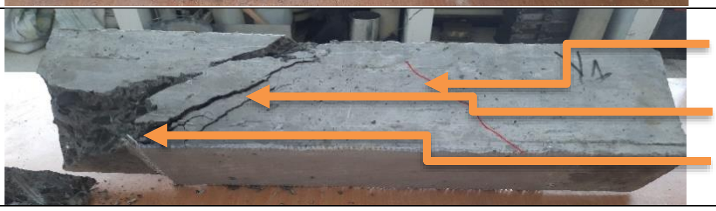	1- Propagation of the shear cracks 2- Shear cracks 3- Debonding of GFRP sheets and crashing of concrete

Beam code	RC Beam concrete	Failure mode
JBJS	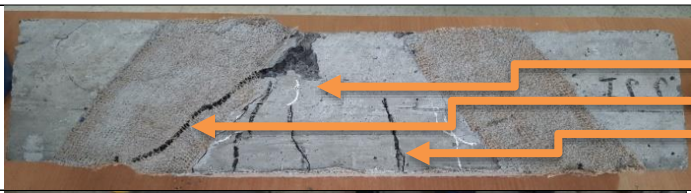	1- Shear cracks 2- Fracture of JFRP sheets 3- Flexural cracks
GBGS		1- Propagation of the shear cracks 2- Shear cracks 3- Debonding of GFRP sheets and crashing of concrete
JBGS (Hybrid reinforcement)		1- Crashing of concrete 2- Debonding of GFRP sheets 3- Flexural cracks
GBJS (Hybrid reinforcement)	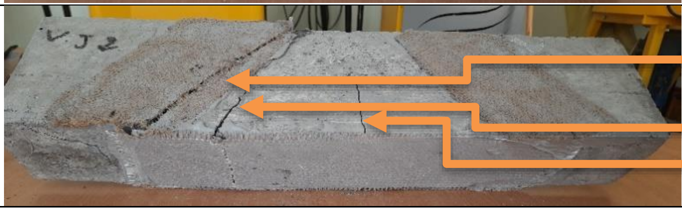	1- Fracture of JFRP and GFRP sheets 2- Shear cracks 3- Flexural cracks

JFRP-reinforced beams (JB and JBJS) exhibited rupture of the jute sheets without prior delamination, indicating effective bonding but early material failure due to the lower tensile capacity of natural fibers. These beams showed more gradual crack propagation and distributed damage.

Hybrid configurations presented mixed failure modes. The JBGS beam (jute at the bottom, glass on the sides) failed by rupture of the jute fibers at mid-span and localized side debonding of the GFRP. In contrast, the GBJS beam (glass at the bottom, jute on the sides) experienced rupture of both fiber types. These hybrid beams exhibited more stable failure progression, with delayed crack growth and better energy absorption than mono-material systems.

4.2. Analysis of Cracking Characteristics

To evaluate the influence of hybrid FRP strengthening on the serviceability of the beams, the cracking characteristics were extracted and analyzed. As summarized in Table 8, the reinforcement configuration significantly influenced the crack distribution and widths.

Table 8. Summary of measured crack characteristics at ultimate load.

Beam code	No. of Cracks	Avg. Crack Spacing (mm)	Avg. Crack Width (mm)	Failure Mode	Typical Literature Ranges
CB	6	185	5.2	Flexural (Concrete crushing)	RC beams: crack spacing ~150–200 mm, crack width ~4–6 mm [71]
GB	4	95	4.2	FRP Debonding	GFRP RC beams: spacing 70–120 mm, width 2–5 mm [71]
JB	5	130	4.9	FRP Rupture	Natural FRP beams: spacing 100–140 mm, width 3–5 mm [72]

Beam code	No. of Cracks	Avg. Crack Spacing (mm)	Avg. Crack Width (mm)	Failure Mode	Typical Literature Ranges
JBJS	8	110	3.8	Hybrid Delamination	Hybrid FRP: spacing 60–120 mm, width 1–4 mm [72]
GBGS	4	100	4.1	Flexural (Concrete crushing)	GFRP-steel hybrid: spacing 70–130 mm, width 2–4.5 mm [73]
JBGS (Hybrid reinforcement)	2	55	2.2	Flexural (Concrete crushing)	Hybrid (natural + glass): spacing 50–80 mm, width 1–2.5 mm [72]
GBJS (Hybrid reinforcement)	3	72	2.5	Flexural (Concrete crushing)	Hybrid (glass + jute): spacing 60–90 mm, width 2–3 mm [72]

The results in Table 8 show that the strengthened beams exhibited reduced crack spacing and widths compared to the control beam (CB), indicating a more efficient distribution of tensile stresses along the span. The hybrid beams demonstrated the most significant improvements, with minimal crack spacing of approximately 55 mm for JBGS and 72 mm for GBJS, and average crack widths of 2.2 mm and 2.5 mm, respectively. These reductions are substantially lower than those of the control and FRP-only beams, suggesting that the combination of Jute and Glass fibers enhances bond-slip behavior and limits the widening of individual flexural cracks.

When compared with literature data, beams reinforced exclusively with FRP, such as GFRP or natural FRP, typically show moderate reductions in crack spacing but relatively larger crack widths due to the lower elastic modulus and bond characteristics of FRP compared to steel. Glass-FRP beams in previous studies exhibited crack spacings of 70 to 120 mm and crack widths of 2 to 5 mm, consistent with the GB beam in this study. Hybrid reinforcement systems that combine FRP with steel or different fiber types have been reported to improve crack control by enhancing load distribution and tension stiffening, often achieving smaller crack widths and spacings than FRP-only beams. The present hybrid configurations (JBJS, JBGS, GBJS, GBGS) follow the same trends, with JBGS and GBJS achieving up to 70 percent reduction in crack spacing and 58 percent reduction in crack width. These results confirm that the proposed hybrid reinforcement schemes effectively improve crack distribution, control crack opening, and enhance the serviceability performance of the beams.

4.3. Load–Deflection Behavior

Figs 5-8 present the load–deflection curves for all beam configurations. The control beam demonstrated the expected elastic–plastic response with a peak load of approximately 49.5 kN. Strengthened beams exhibited increased stiffness and load capacity, with varying levels of post-yield deformation.

Fig. 7 shows that GB (GFRP-bottom-only) reached a peak load of 63.7 kN, a 29% increase over the control, with moderate deflection. JB (JFRP-bottom-only) showed a more ductile profile but a lower peak load of 56.1 kN, representing only a 13% strength gain. As seen in Fig. 8, U-wrapped beams exhibited superior performance. GBGS (GFRP on bottom and sides) reached 71.3 kN (44% improvement), while JBJS (JFRP on bottom and sides) achieved 68.3 kN (38% gain). Both showed improved deflection over bottom-only counterparts, with JBJS being more ductile. Hybrid systems, illustrated in Fig. 9, demonstrated balanced structural behavior. JBGS achieved a load of 63.3 kN and the highest deflection (20.4 mm), showing strong energy dissipation. GBJS reached 59.9 kN with intermediate deformability.

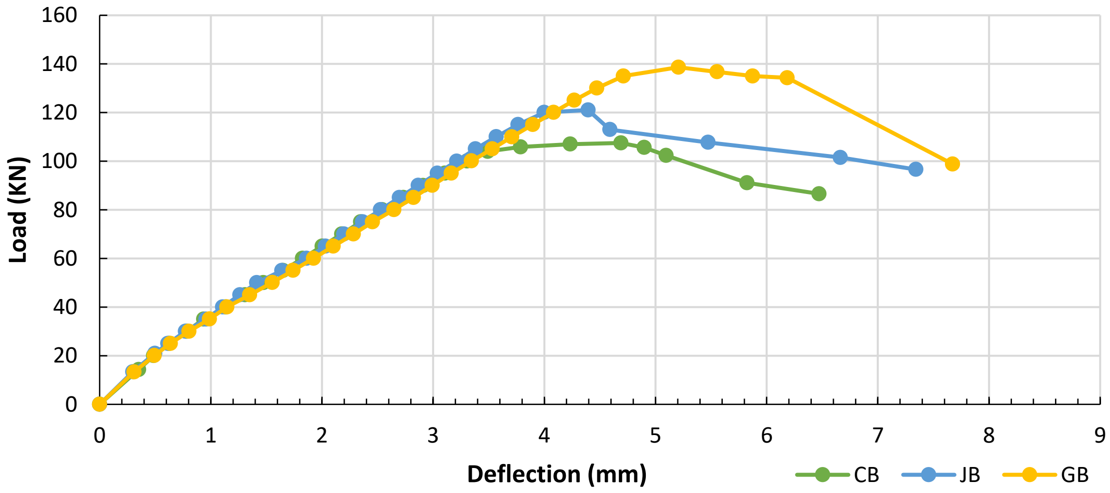

Fig. 7. Load–deflection curves for beams strengthened only at the bottom face, compared to the unstrengthened control beam

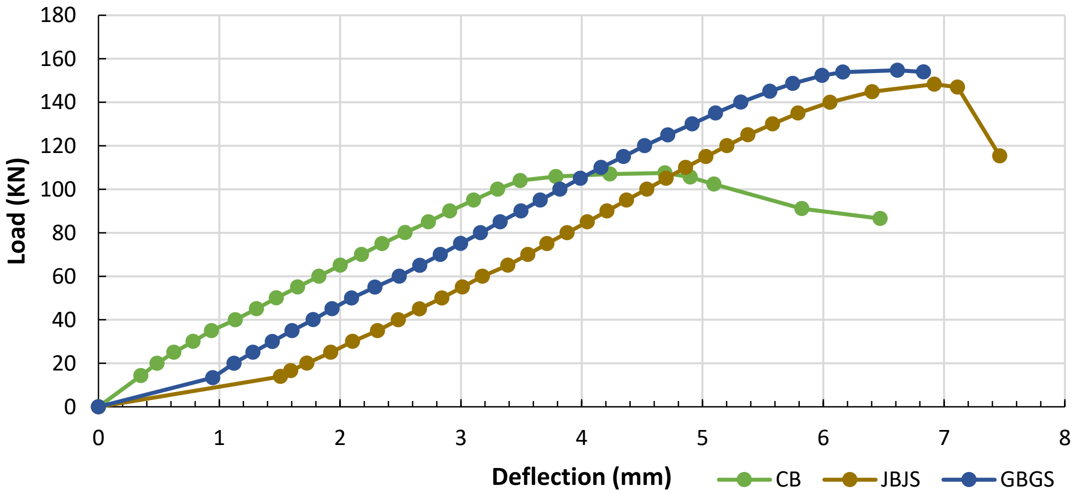

Fig. 8. Load–deflection curves for beams strengthened on the bottom and side faces using the same FRP type, compared to the control beam

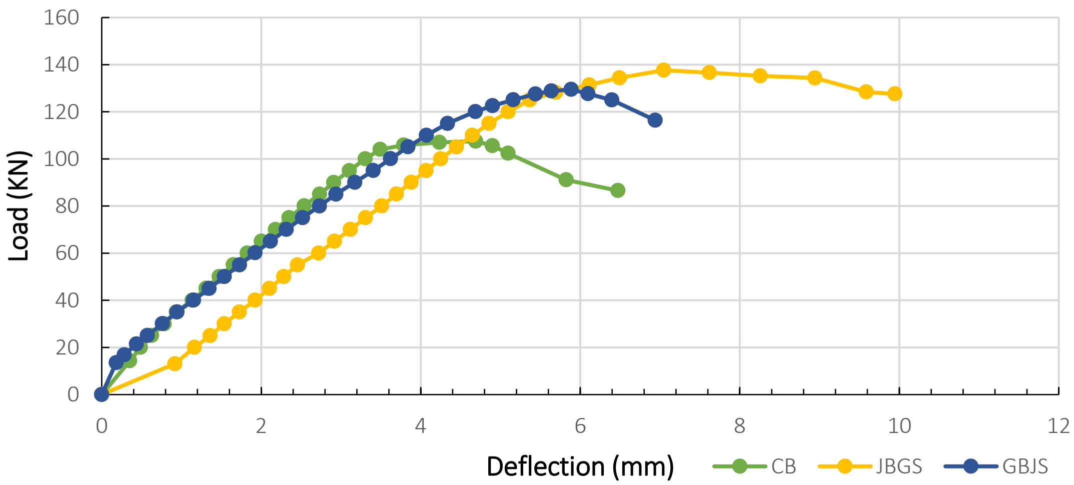

Fig. 9. Load–deflection curves for hybrid-strengthened beams (GFRP and JFRP in combined configurations), compared to the control beam

4.4. Ultimate Load Performance

The percentage gains in peak load relative to the control beam are presented in Fig. 10 and quantified in Table 9. The GBGS beam exhibited the highest increase (44%), followed by JBJS (38%), JBGS (28%), GB (29%), and GBJS (21%). The JB beam showed the lowest gain at 13%.

Table 9. Summary of mechanical performance parameters including ultimate load, and mid-span deflection, for all strengthened and control RC beams, with percentage gains to evaluate strengthening efficiency.

Beams	f_u (kN)	f_{us} (kN)	δ_u (mm)	δ_{us} (mm)	$\frac{f_{us}-f_u}{f_u}$ (%)	$\frac{\delta_{us}-\delta_u}{\delta_u}$ (%)
CB	107.5	/	4.68	/	/	/
JB	/	121.7	/	4.4	+13	-6
GB	/	138.6	/	5.2	+29	+11
JBJS	/	148.3	/	6.92	+38	+47
GBGS	/	154.7	/	6.61	+44	+41
JBGS	/	137.6	/	7.04	+28	+50
GBJS	/	129.6	/	5.88	+21	+25

As shown in Table 9, although GFRP has a higher ultimate deformation capacity, the inclusion of JFRP layers in the hybrid configuration (JBGS, GBJS) resulted in a more uniform crack distribution and a gradual loss of stiffness prior to failure. This suggests that JFRP acts as a 'sacrificial' or 'shock-absorbing' component that prevents the catastrophic and explosive delamination often associated with pure GFRP reinforcement. These results confirm that U-wrap configurations significantly enhance flexural strength by improving anchorage and stress redistribution. Hybrid systems demonstrated comparable gains to synthetic FRPs, validating the contribution of natural fibers when placed in strategic locations.

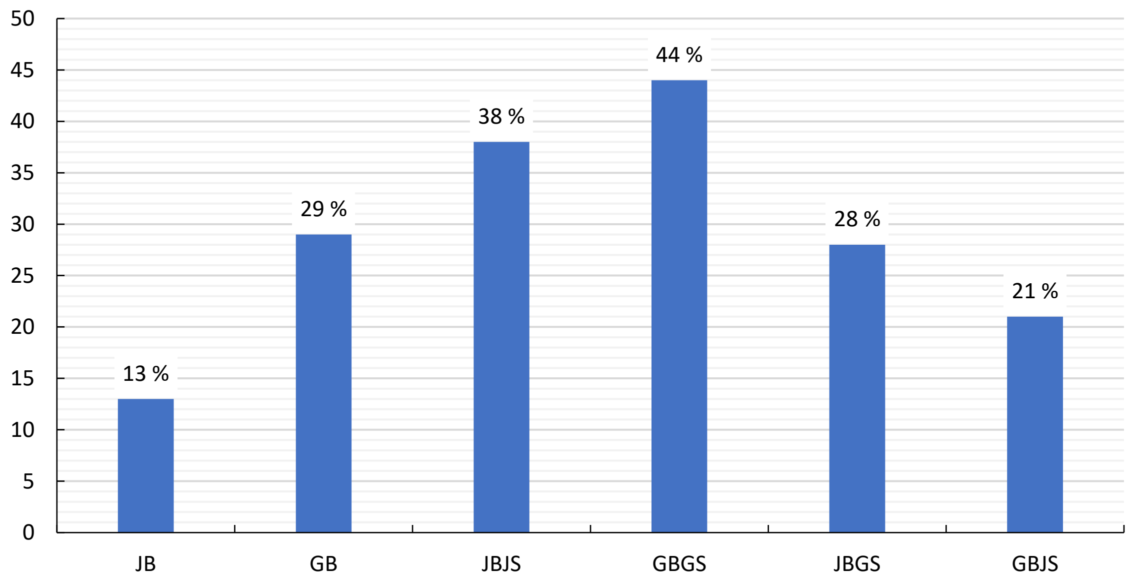

Fig. 10. Percentage improvement in ultimate load for all FRP-strengthened beams compared to the control

The mechanical superiority of the JBGS system over the GBJS and mono-material configurations can be attributed to optimized strain compatibility and stress redistribution. In the JBGS layout, the high-modulus GFRP side layers act as a stiff 'anchorage frame' that stabilizes the JFRP soffit, effectively delaying the onset of interfacial debonding. This configuration facilitates a more uniform stress transfer across the concrete-FRP interface, allowing the jute fibers to reach higher strain levels before failure. In contrast, the GBJS system lacks this external confinement, leading to localized stress concentrations and premature delamination. This anchorage effect in the JBGS specimens transforms the failure mode from a sudden, brittle loss of bond to a controlled, pseudo-ductile response, explaining the substantial 71% increase in the ductility index.

4.5. Analytical Evaluation of Hybrid Synergy

To quantitatively define the "synergy" observed in the hybrid configurations, a Synergy Index (S_{yn}) was implemented. This analytical approach evaluates whether the hybrid system performs better than the theoretical sum of its individual components. The index is derived from the Rule of Mixtures (RoM) as follows:

$$S_{yn} = \frac{P_{exp\ (hybrid)}}{\sum P_i V_i} \tag{1}$$

Where; $P_{exp\ (hybrid)}$ is the experimental ultimate load of the hybrid specimen (e.g., JBGS or GBJS), P_i represents the ultimate load of the mono-material reference beams strengthened at the bottom (GB for glass and JB for jute), V_i is the relative contribution of each fiber type (taken as 0.5 for the hybrid configurations).

As shown in Table 9, the theoretical benchmark for the hybrid systems, calculated as the average of GB (138.6 kN) and JB (121.7 kN), is 130.15 kN. The JBGS configuration (Jute bottom + Glass sides) achieved an experimental ultimate load of 137.6 KN, resulting in a Synergy Index of 1.057. This value, being greater than 1.0, provides analytical evidence of a positive synergistic effect. It demonstrates that the strategic spatial positioning of glass fibers as side reinforcement prevents the premature debonding of the jute fibers on the bottom face, allowing the hybrid system to exceed its theoretical additive capacity. This quantitative result analytically confirms the "synergy" mentioned throughout this study. The side reinforcement (Glass in JBGS) acts not just as additional strength, but as a protective mechanism that restrains the dilation of the concrete and prevents the premature debonding of the jute fibers on the bottom face, resulting in a system that is more resilient than the sum of its parts.

4.6. Mid-Span Deflection at Ultimate Load

Fig. 11 shows the improvement in mid-span deflection across all beams. JBGS recorded the highest deflection gain (50%), followed by JBJS (47%) and GBGS (41%). GB and GBJS reached 11% and 25% respectively, while JB surprisingly exhibited a 6% reduction, attributed to premature fiber rupture without sufficient anchorage. These findings highlight the ability of hybrid and U-wrapped systems to improve deformability. JBGS, in particular, combined a ductile failure mechanism with increased capacity, offering improved serviceability and resilience.

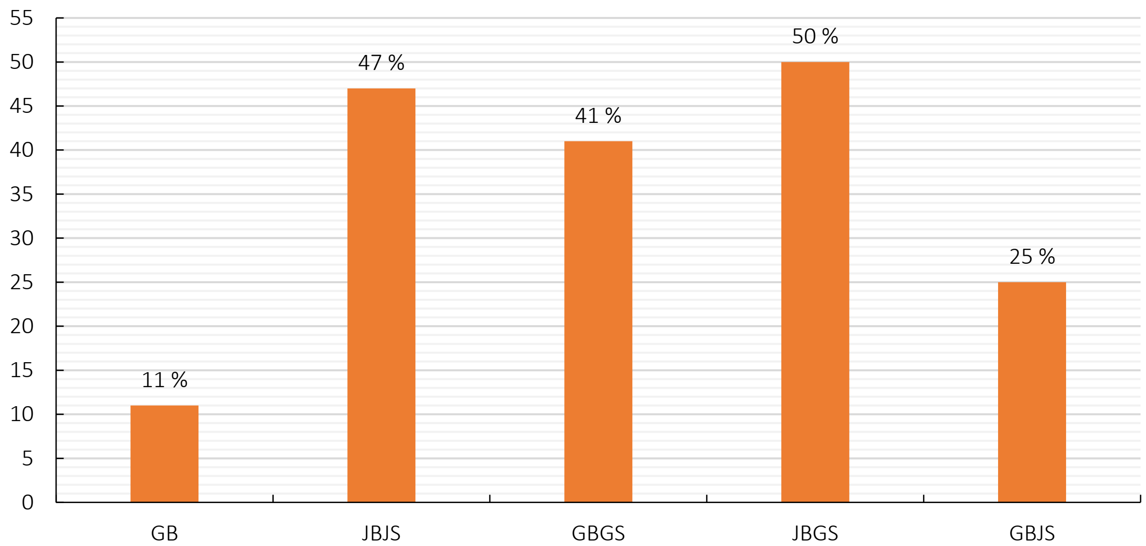

Fig. 11. Percentage increase in mid-span deflection at peak load for all strengthened beams relative to the control beam

4.7. Ductility Index

The ductility index (μ), defined as the area under the load–deflection curve normalized to the control beam, is summarized in Fig. 12 and Table 9. The GBGS beam achieved the highest gain in ductility index (86%), followed by JBJS (80%), GB (78%), JBGS (71%), and JB (62%). GBJS reached 60%, slightly lower due to its stiffer GFRP base and early jute rupture. To quantify the ability of the hybrid JFRP/GFRP system to sustain inelastic deformation, the ductility index (μ) was calculated for all specimens. This index is defined as the ratio of the displacement at the ultimate load to the displacement at the first yielding of the internal longitudinal steel reinforcement, as shown in the following equation:

$$\mu = \frac{\delta_u}{\delta_y} \tag{2}$$

Where; δ_u is the ultimate displacement, δ_y is the yield displacement.

These results confirm that U-shaped and hybrid systems not only improve ultimate strength but also significantly enhance energy absorption and post-yield deformation. The JBGS configuration, in particular, provides an optimal balance between stiffness and ductility. The superior performance of the JBGS configuration compared to GBJS is attributed to the optimized layering sequence that enhances strain compatibility and interfacial stress transfer. In the JBGS system, the inner Jute layer acts as a compliant buffer that uniformly distributes concrete expansion and micro-cracking, allowing the high-stiffness outer Glass layer to reach its ultimate capacity more effectively. This creates a synergetic, multi-stage failure mode that significantly increases energy dissipation and results in a 71% ductility gain. Conversely, in the GBJS setup, the high-stiffness Glass fibers are placed in direct contact with the concrete, subjecting them to localized stress concentrations and premature brittle failure. Because the outer Jute layer in GBJS remains at a lower tension state when the internal Glass layer fractures, the system fails to achieve the same "Hybrid Effect," leading to reduced structural resilience and lower overall ductility.

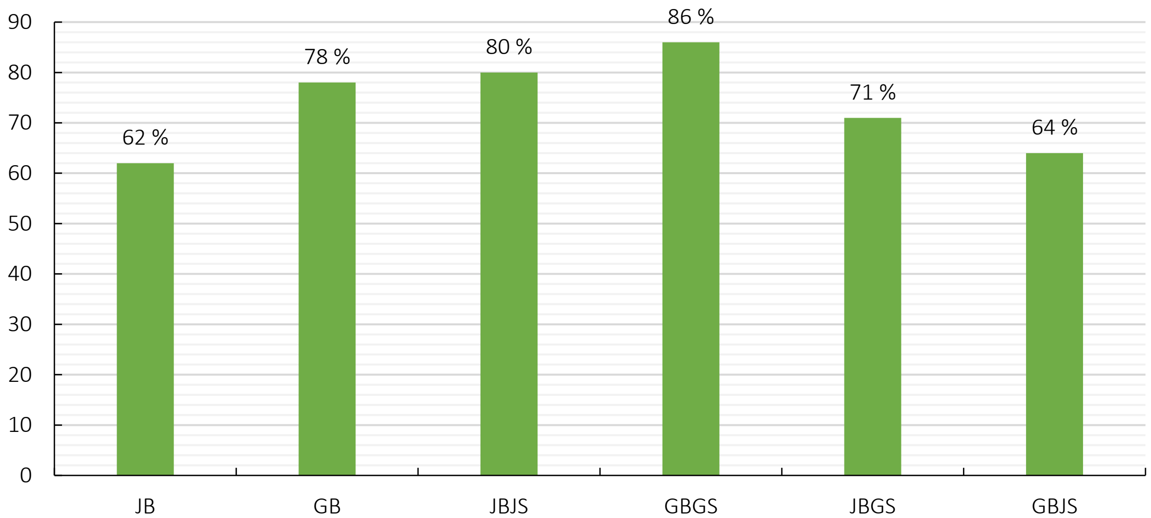

Fig. 12. Percentage gain in ductility index for all strengthened beams compared to the unstrengthened referenc.

The ductility of the strengthened beams was evaluated using an energy-based index, defined as the ratio of total energy absorption to elastic energy.

$$E_D = \frac{\int_0^{\delta_u} P(\delta)\, d\delta}{\frac{1}{2} P_y \delta_y} \tag{3}$$

This method was chosen over traditional displacement-based indices because the hybrid GFRP/JFRP system exhibits a pseudo-ductile, multi-stage failure rather than a single discrete yield point. Physically, this index represents the capacity of the hybrid configuration to dissipate energy through progressive fiber micro-cracking and controlled interfacial slip. While this approach effectively captures the toughening effect of the jute fibers, its limitation lies in the sensitivity to the post-peak slope; the index may over-estimate ductility if a significant residual load is maintained despite extensive structural damage.

The enhanced performance of the hybrid system is fundamentally rooted in fiber modulus heterogeneity. By combining high-modulus Glass fibers with lower-modulus Jute fibers, a staggered mechanical activation is achieved. Initially, the stiffer Glass fibers bear the majority of the load, providing the necessary stiffness to arrest micro-cracks. As the system approaches peak strain, the modulus mismatch allows the more compliant Jute fibers to continue dissipating energy and bridging macro-cracks even after the Glass fibers begin to fracture. This heterogeneity prevents a sudden, brittle catastrophic failure, instead facilitating a progressive 'pseudo-ductile' response that explains the 71% increase in the ductility index for the JBGS configuration.

4.8. Evaluation of Elastic Stiffness

The elastic stiffness (K) was evaluated to determine the influence of the strengthening configuration on the structural rigidity of the beams during the serviceability stage. The stiffness is defined as the slope of the load-deflection curve within the linear elastic range:

$$K = \frac{\Delta P}{\Delta \delta} \tag{4}$$

Where ΔP and $\Delta \delta$ represent the increment in load and mid-span deflection, respectively, prior to the yielding of the internal steel reinforcement. The results are summarized in Table 10.

Table 10. Elastic stiffness of plain steel and FRP-strengthened beams

Beam Designation	Strengthening Configuration	Elastic Stiffness (kN/mm)	Increase/decrease over Control (%)
CB	None (Control)	22.97	—
GB	GFRP	26.65	16.1%
JB	JFRP	27.66	20.42%
JBJS	JFRP	21.43	-7.08%
GBGS	Hybrid	23.4	1.87%
JBGS	Hybrid	19.54	-17.55%
GBJS	Hybrid	22.05	-4.17%

As shown in Table 10, the impact of FRP strengthening on elastic stiffness varied significantly depending on the fiber type and layout. The JB specimen exhibited the highest stiffness enhancement of 20.42%, followed closely by the GB specimen at 16.1%. Among the hybrid configurations, GBGS showed a slight improvement of 1.87%, effectively maintaining the rigidity of the control beam while providing the benefits of hybridization.

Conversely, the JBGS and JBJS configurations showed a reduction in initial stiffness of 17.55% and 7.08%, respectively. This decrease in the linear-elastic slope suggests that the specific arrangement of jute and glass layers in these specimens may have introduced a slight increase in initial compliance or localized micro-cracking during the early loading stages before the FRP contribution was fully mobilized. Despite these variations in the serviceability range, these configurations ultimately contributed to significant gains in ultimate capacity and ductility as discussed in previous sections.

5. Conclusions

This study experimentally evaluated the flexural behavior of reinforced concrete beams externally strengthened with GFRP, JFRP, and hybrid GFRP–JFRP systems. Fourteen beams were tested under four-point bending to assess the effects of fiber type, layout configuration, and positioning on strength, deformability, and failure mode. Based on the analysis of load–deflection behavior, failure patterns, and ductility, the following conclusions can be drawn:

- GFRP-based U-wrap reinforcement (GBGS) provided the highest strength gain, with a 44% increase in ultimate load relative to the control beam.
- The JBJS (JFRP U-wrap) configuration demonstrated a 38% increase in strength and the second-highest ductility, highlighting the effectiveness of natural fibers when provided with proper anchorage.
- The JBGS (jute bottom, glass sides) hybrid system achieved a 28% increase in load capacity, a 50% gain in deflection, and a 71% rise in ductility index, identifying it as the most balanced and resilient system tested.
- Failure modes were significantly affected by fiber type and positioning. GFRP systems were prone to debonding, JFRP systems failed by fiber rupture, while hybrid systems exhibited mixed and more stable failure behavior.
- U-shaped configurations improved both strength and deformability by enhancing confinement and delaying premature debonding, especially in hybrid reinforcements.

The results confirm that hybrid GFRP–JFRP systems, when strategically arranged, can achieve competitive performance compared to fully synthetic systems while introducing ductility and sustainability advantages. This approach offers a viable, eco-efficient alternative for structural strengthening applications in civil infrastructure, including beams, slabs, and pavement substructures.

Despite the significant performance gains observed in the JBJS and JBGS configurations, several limitations of the current study should be acknowledged to guide future investigations:

- Long-term Durability: Investigation is needed on JFRP degradation under environmental stressors like moisture, UV, and concrete alkalinity.
- Cyclic Loading: Testing under fatigue and seismic-type loading is required to verify the hybrid system's performance in infrastructure applications.
- Bond-Slip Behavior: Micro-scale analysis of the hybrid FRP-to-concrete interface is necessary to better define debonding mechanisms.
- Size Effect: Validation on larger-scale structural elements is recommended to confirm the scalability of the JBGS configuration.

Future investigations should incorporate standardized pull-off and bond–slip testing to characterize the interfacial constitutive laws and develop analytical load transfer models that account for the complex stress distribution between synthetic and natural fiber layers. Furthermore, to transition current qualitative sustainability claims into demonstrated outcomes, future research must include Life Cycle Assessments (LCA) to provide quantitative environmental indicators and durability testing under accelerated aging to evaluate the long-term performance of jute fibers. Additionally, exploring the use of bio-based resins in place of traditional epoxies could further optimize the eco-efficiency of the system, aligning with the growing demand for fully sustainable structural rehabilitation.

Future research should focus on long-term durability under environmental exposure, fatigue resistance under cyclic loads, and the development of predictive models for hybrid FRP systems. Optimization of fiber orientation, layer thickness, and anchorage details will be essential for translating these findings into standardized design guidelines.

Nomenclature

Symbol	Description	Unit
a/b	Shear span-to-effective depth ratio	—
E_c	Modulus of elasticity of concrete	GPa
K	Elastic stiffness	kN /mm
M_n	Nominal flexural strength	kN ·m
P_u	Ultimate load capacity	kN
V_n	Nominal shear strength	kN

Symbol	Description	Unit
δ_u	Mid-span deflection at ultimate load	mm
δ_y	Mid-span deflection at steel yielding	mm
μ	Ductility index	—
E_D	Energy-based ductility index	—
ρ	Reinforcement ratio	%
ΔP	Change in applied load	kN
$\Delta\delta$	Change in deflection	kN
S_{yn}	Synergy Index	—
$P_{exp\ (hybrid)}$	Experimental ultimate load of the hybrid specimen	kN
P_i	Ultimate load	kN
V_i	Relative contribution of each fiber type	kN

References

[1] Mosley WH, Bungey JH, Hulse R. Reinforced concrete design. Springer; 1999. https://doi.org/10.1007/978-1-349-14911-7
[2] Wight JK, MacGregor JG. Reinforced concrete. Pearson Education UK Sydney, NSW; 2016.
[3] Chatbi M, et al. Nano-Clay Platelet Integration for Enhanced Bending Performance of Concrete Beams Resting on Elastic Foundation: An Analytical Investigation. Materials. 2023;16(14):5040. https://doi.org/10.3390/ma16145040
[4] Kecir A, Chatbi M, Harrat ZR, Bouiadjra MB, Bouremana M, Krour B. Enhancing the Mechanical Performance of Concrete Slabs through the Incorporation of Nano-sized Iron Oxide Particles (Fe2O3): Non-local Bending Analysis. Periodica Polytechnica Civil Engineering. 2024;68(3):842-858. https://doi.org/10.3311/PPci.23016
[5] Reynolds CE, Steedman JC, Threlfall AJ. Reinforced concrete designer's handbook. CRC Press; 2007.
[6] Benfrid A, Benbakhti A, Harrat ZR, Chatbi M, Krour B, Bouiadjra MB. Thermomechanical Analysis of Glass Powder Based Eco-concrete Panels: Limitations and Performance Evaluation. Periodica Polytechnica Civil Engineering. 2023;67(4):1284-1297. https://doi.org/10.3311/PPci.22781
[7] Delatte N. Concrete pavement design, construction, and performance. CRC Press; 2018. https://doi.org/10.1201/9781482288483
[8] Hassoun MN, Al-Manaseer A. Structural concrete: theory and design. John Wiley & Sons; 2020.
[9] Chatbi M, Krour B, Benatta MA, Harrat ZR, Amziane S, Bouiadjra MB. Bending analysis of nano-SiO2 reinforced concrete slabs resting on elastic foundation. Structural Engineering and Mechanics, An Int'l Journal. 2022;84(5):685-697.
[10] Harrat ZR, et al. Modeling the Thermoelastic Bending of Ferric Oxide (Fe2O3) Nanoparticles-Enhanced RC Slabs. Materials. 2023;16(8):3043. https://doi.org/10.3390/ma16083043
[11] Benfrid A, Chatbi M, Harrat ZR, Bouiadjra MB. Selective Integration of Waste-Derived Glass Nanopowders in Structural Wall Concrete: Improving Thermal Efficiency and Elasto-Mechanical Properties for Sustainable Construction. Periodica Polytechnica Civil Engineering. 2025;69(3):954-965. https://doi.org/10.3311/PPci.39913
[12] Mehta PK. Concrete: Structure, properties and materials. 1986.
[13] De Schutter G. Damage to concrete structures. Taylor & Francis; 2017. https://doi.org/10.1201/b12914
[14] Harrat ZR, et al. Bending analysis of nano-Fe2O3 reinforced concrete slabs exposed to temperature fields and supported by viscoelastic foundation. Advances in Concrete Construction. 2024;17(2):111-126.
[15] Woodson RD. Concrete structures: protection, repair and rehabilitation. Butterworth-Heinemann; 2009.
[16] Modi PI, Patel CN. Repair and Rehabilitation of Concrete Structures. PHI Learning Pvt. Ltd.; 2015.
[17] Asmara YP. Concrete Reinforcement Degradation and Rehabilitation: Damages, Corrosion and Prevention. Springer Nature; 2023. https://doi.org/10.1007/978-981-99-5933-4
[18] Moulay-Ali A, Abdeldjalil M, Khelafi H. An experimental study on the optimal compositions of ordinary concrete based on corrected dune sand-Case of granular range of 25 mm. Case Studies in Construction Materials. 2021;14:e00521. https://doi.org/10.1016/j.cscm.2021.e00521
[19] Benbakhti A, Benfrid A, Harrat ZR, Chatbi M, Bouiadjra MB, Krour B. An Analytical Analysis of the Hydrostatic Bending to Design a Wastewater Treatment Plant by a New Advanced Composite Material. Journal of Composite & Advanced Materials/Revue des Composites et des Matériaux Avancés. 2024;34(2):177-188. https://doi.org/10.18280/rcma.340207
[20] Dine Elhennani S, et al. Buckling and Free Vibration Analyses of Various Nanoparticle Reinforced Concrete Beams Resting on Multi-Parameter Elastic Foundations. Materials. 2023;16(17). https://doi.org/10.3390/ma16175865

[21] Thirupathi S, Palanisamy S, Asokan V. Enhancing sustainability in construction: Exploring the self-healing mechanisms of bio-concrete. Res Eng Struct Mater. 2025;11(6):2731-2744. https://doi.org/10.17515/resm2025-517ma1105rs
[22] Sreadha AR, Pany C, Varkey MV. A Review on Seismic Retrofit of Beam-Column Joints. International Journal for Modern Trends in Science and Technology. 2020;6(9):80-93. https://doi.org/10.46501/IJMTST060914
[23] Sangeetha P, Prithvi R, Ashwin KV, Murali B, Yaashika M. Structural behavior of deficient hollow steel columns strengthened using GFRP. Res Eng Struct Mater. 2025;11(6):2745-2760. https://doi.org/10.17515/resm2025-541st1121rs
[24] Van Den Einde L, Zhao L, Seible F. Use of FRP composites in civil structural applications. Construction and Building Materials. 2003;17(6-7):389-403. https://doi.org/10.1016/S0950-0618(03)00040-0
[25] Belarbi A, Dawood M, Acun B. Sustainability of fiber-reinforced polymers (FRPs) as a construction material. In: Sustainability of construction materials. Elsevier; 2016. p. 521-538. https://doi.org/10.1016/B978-0-08-100370-1.00020-2
[26] Hota G, Liang R. Advanced fiber reinforced polymer composites for sustainable civil infrastructures. In: Proceedings of the International Symposium on Innovation & Sustainability of Structures in Civil Engineering; 2011; Xiamen University.
[27] Alzate A, Arteaga Á, de Diego A, Perera R. Shear strengthening of reinforced concrete beams using fibre reinforced polymers (FRP). European Journal of Environmental and Civil Engineering. 2009;13(9):1051-1060. https://doi.org/10.1080/19648189.2009.9693172
[28] Maraveas C, Miamis K, Vrakas AA. Fiber-reinforced polymer-strengthened/reinforced concrete structures exposed to fire: A review. Structural Engineering International. 2012;22(4):500-513. https://doi.org/10.2749/101686612X13363929517613
[29] Aouadi A, Ghernouti Y. Comportament flexibil-forfecare a grinzilor de beton armat Întărit de diverse rețele de compozite încorporate. Revista Romana de Inginerie Civila. 2020;11(2):196-207. https://doi.org/10.37789/rjce.2020.11.2.4
[30] Frih A, et al. A novel hyperbolic integral-Quasi-3D theory for flexural response of laminated composite plates. Geomechanics and Engineering. 2023;34(3):233-250.
[31] Chatbi M, Harrat ZR, Ghazoul T, Bouiadjra MB. Free vibrational analysis of composite beams reinforced with randomly aligned and oriented carbon nanotubes, resting on an elastic foundation. Journal of Building Materials and Structures. 2022;9(1):22-32. https://doi.org/10.34118/jbms.v9i1.1895
[32] Lakhder M, Benfrid A, Bouiadjra MB, Chatbi M, Harrat ZR, Benbakhti A. The Mechanical Bending Behavior of a New Metal Alloy Nano-Reinforced Plate Incorporating Tungsten Nanoparticles. NIPES - Journal of Science and Technology Research. 2025;7(3):423-440. https://doi.org/10.37933/nipes/7.3.2025.1682
[33] Sreadha AR, Pany C. Static, Free Vibration and Buckling Analysis of Composite Panels; A Review. Advanced Journal of Graduate Research. 2020;9(1):21-45. https://doi.org/10.21467/ajgr.9.1.21-45
[34] Ramesh B, Eswari S, Sundararajan T. Flexural behaviour of glass fibre reinforced polymer (GFRP) laminated hybrid-fibre reinforced concrete beams. SN Applied Sciences. 2020;2(2):204. https://doi.org/10.1007/s42452-020-1966-2
[35] Iskender M, Karasu B. Glass fibre reinforced concrete (GFRC). El-Cezerî Fen ve Mühendislik Dergisi. 2018;5(1):136-162. https://doi.org/10.31202/ecjse.371950
[36] Aslani F, Gunawardena Y, Dehghani A. Behaviour of concrete filled glass fibre-reinforced polymer tubes under static and flexural fatigue loading. Construction and Building Materials. 2019;212:57-76. https://doi.org/10.1016/j.conbuildmat.2019.03.321
[37] Correia JR. Fibre-reinforced polymer (FRP) composites. In: Materials for construction and civil engineering: science, processing, and design. Springer; 2014. p. 501-556. https://doi.org/10.1007/978-3-319-08236-3_11
[38] Lee SW, Hong KJ, Park S. Current and future applications of glass-fibre-reinforced polymer decks in Korea. Structural Engineering International. 2010;20(4):405-408. https://doi.org/10.2749/101686610793557672
[39] Frigione M, Lettieri M. Durability issues and challenges for material advancements in FRP employed in the construction industry. Polymers. 2018;10(3):247. https://doi.org/10.3390/polym10030247
[40] Zaman A, Gutub SA, Wafa MA. A review on FRP composites applications and durability concerns in the construction sector. Journal of Reinforced Plastics and Composites. 2013;32(24):1966-1988. https://doi.org/10.1177/0731684413492868
[41] Wu Z, Wang X, Zhao X, Noori M. State-of-the-art review of FRP composites for major construction with high performance and longevity. International Journal of Sustainable Materials and Structural Systems. 2014;1(3):201-231. https://doi.org/10.1504/IJSMSS.2014.062757

[42] Chen C, et al. Comparative analysis of natural fiber reinforced polymer and carbon fiber reinforced polymer in strengthening of reinforced concrete beams. Journal of Cleaner Production. 2020;263:121572. https://doi.org/10.1016/j.jclepro.2020.121572
[43] Ahamed MS, Ravichandran P, Krishnaraja A. Natural fibers in concrete-A review. In: IOP Conference Series: Materials Science and Engineering. IOP Publishing; 2021. vol. 1055, no. 1, p. 012038. https://doi.org/10.1088/1757-899X/1055/1/012038
[44] Yan L, Chouw N. Natural FRP tube confined fibre reinforced concrete under pure axial compression: A comparison with glass/carbon FRP. Thin-Walled Structures. 2014;82:159-169. https://doi.org/10.1016/j.tws.2014.04.013
[45] Abdelhak A, Abdelkader F, Fakhreddine D, Imene B, Adel D, Chebabhi L. Reduce energy consumption by using glass fiber reinforced concrete. Brazilian Applied Science Review. 2024;8(2):e74713. https://doi.org/10.34115/basrv8n2-019
[46] Sreadha AR, Pany C. Review on Fabrication of Bamboo Composite Materials Reinforced Concrete. Journal of Science & Technology. 2020;5(3):258-279. https://doi.org/10.46243/jst.2020.v5.i3.pp258-279
[47] Islam MS, Ahmed SJ. Influence of jute fiber on concrete properties. Construction and Building Materials. 2018;189:768-776. https://doi.org/10.1016/j.conbuildmat.2018.09.048
[48] Zakaria M, Ahmed M, Hoque MM, Islam S. Scope of using jute fiber for the reinforcement of concrete material. Textiles and Clothing Sustainability. 2016;2(1):11. https://doi.org/10.1186/s40689-016-0022-5
[49] Tan H, Yan L, Huang L, Wang Y, Li H, Chen JY. Behavior of sisal fiber concrete cylinders externally wrapped with jute FRP. Polymer Composites. 2017;38(9):1910-1917. https://doi.org/10.1002/pc.23761
[50] Zakaria M, Ahmed M, Hoque M, Shaid A. A comparative study of the mechanical properties of jute fiber and yarn reinforced concrete composites. Journal of Natural Fibers. 2020.
[51] Gulzar MA, et al. Influence of jute fiber on tensile, electrical, and permeability characteristics of slag concrete: a better, cheaper, and eco-friendly substitute for conventional concrete. Journal of Natural Fibers. 2023;20(1):2170947. https://doi.org/10.1080/15440478.2023.2170947
[52] Idder A, Hamouine A, Labbaci B, Abdeldjebar R. The porosity of stabilized earth blocks with the addition plant fibers of the date palm. Civil Engineering Journal. 2020;6(3):478-494. https://doi.org/10.28991/cej-2020-03091485
[53] Khan MB, et al. Effects of jute fiber on fresh and hardened characteristics of concrete with environmental assessment. Buildings. 2023;13(7):1691. https://doi.org/10.3390/buildings13071691
[54] Pradeep P, Dhas JER, Ramachandran M, Retnam BSJ. Mechanical Characterization of jute fiber over glass and carbon fiber reinforced polymer composites. International Journal of Applied Engineering Research. 2015;10(11):10392-10396.
[55] Sridhar J, Gobinath R, Kırgız MS. Comparative study for efficacy of chemically treated jute fiber and bamboo fiber on the properties of reinforced concrete beams. Journal of Natural Fibers. 2022;19(15):12224-12234. https://doi.org/10.1080/15440478.2022.2054894
[56] Ahmad J, Arbili MM, Majdi A, Althoey F, Deifalla AF, Rahmawati C. Performance of concrete reinforced with jute fibers (natural fibers): A review. Journal of Engineered Fibers and Fabrics. 2022;17:15589250221121871. https://doi.org/10.1177/15589250221121871
[57] Akid ASM, Wasiew QA, Sobuz MHR, Rahman T, Tam VW. Flexural behavior of corroded reinforced concrete beam strengthened with jute fiber reinforced polymer. Advances in Structural Engineering. 2021;24(7):1269-1282. https://doi.org/10.1177/1369433220974783
[58] Varma DA, Sarker PK, Madhavan MK, Jayanarayanan K. Experimental and analytical assessment of strengthening of concrete cylinders using jute/basalt hybrid textile fiber reinforced mortar. In: Structures. Elsevier; 2024. vol. 70, p. 107807. https://doi.org/10.1016/j.istruc.2024.107807
[59] Maciel LP, et al. Experimental Analysis of Shear-Strengthened RC Beams with Jute and Jute-Glass Hybrid FRPs Using the EBR Technique. Buildings. 2024;14(9):2893. https://doi.org/10.3390/buildings14092893
[60] Benaddache L, et al. Comparative study on externally bonded heat-treated jute and glass fiber reinforcement for repair of pre-cracked high performance concrete beams. Archives of Civil and Mechanical Engineering. 2024;24(2):82. https://doi.org/10.1007/s43452-024-00899-5
[61] Sen T, Reddy HJ. Strengthening of RC beams in flexure using natural jute fibre textile reinforced composite system and its comparative study with CFRP and GFRP strengthening systems. International Journal of Sustainable Built Environment. 2013;2(1):41-55. https://doi.org/10.1016/j.ijsbe.2013.11.001
[62] Djeddi F, Ghernouti Y, Abdelaziz Y, Alex L. Strengthening in flexure-shear of RC beams with hybrid FRP systems: Experiments and numerical modeling. Journal of Reinforced Plastics and Composites. 2016;35(22):1642-1660. https://doi.org/10.1177/0731684416662532
[63] Nurazzi N, et al. A review on mechanical performance of hybrid natural fiber polymer composites for structural applications. Polymers. 2021;13(13):2170. https://doi.org/10.3390/polym13132170

[64] Ribeiro F, Correia L, Sena-Cruz J. Hybridization in FRP composites for construction: State-of-the-art review and trends. Journal of Composites for Construction. 2024;28(4):04024024. https://doi.org/10.1061/JCCOF2.CCENG-4486
[65] Alabi OO, Olaleye AO, Akande TO, Gbadeyan OJ, Fasina AO. Advanced engineering applications of natural fiber composites for wind turbine blades. Sustainable Smart Composites. 2025;67-86. https://doi.org/10.1201/9781003527275-4
[66] Hason MM, Hanoon AN, Saleem SJ, Hejazi F, Al Zand AW. Characteristics of experimental ductility energy index of hybrid-CFRP reinforced concrete deep beams. SN Applied Sciences. 2021;3(2):200. https://doi.org/10.1007/s42452-021-04202-6
[67] Harris HG, Somboonsong W, Ko FK. New ductile hybrid FRP reinforcing bar for concrete structures. Journal of Composites for Construction. 1998;2(1):28-37. https://doi.org/10.1061/(ASCE)1090-0268(1998)2:1(28)
[68] V BK, M CCH, Lingeshwaran N, S KI. Structural application of fiber reinforced concrete. Res Eng Struct Mater. 2025;11(5):1913-1946. http://dx.doi.org/10.17515/resm2024.305st0531rs
[69] Chatbi M, Lozančić S, Harrat ZR, Hadzima-Nyarko M. Computational Models for the Vibration and Modal Analysis of Silica Nanoparticle-Reinforced Concrete Slabs with Elastic and Viscoelastic Foundation Effects. Modelling. 2026;7(1):8. https://doi.org/10.3390/modelling7010008
[70] Comité Européen de Normalisation. Eurocode 2: Design of concrete structures-Part 1-1: General rules and rules for buildings. London: British Standard Institution; 2004. p. 37.
[71] Barris C, Torres L, Vilanova I, Miàs C, Llorens M. Experimental study on crack width and crack spacing for Glass-FRP reinforced concrete beams. Engineering Structures. 2017;131:231-242. https://doi.org/10.1016/j.engstruct.2016.11.007
[72] Alsuhaibani E, Aldukail A. Experimental Study on Hybrid Steel-GFRP Reinforced Concrete Beams with Different Stirrup Types and Spacings. Buildings. 2025;15(22):4047. https://doi.org/10.3390/buildings15224047
[73] Bui LVH, Stitmannaithum B, Ueda T. Ductility of concrete beams reinforced with both fiber-reinforced polymer and steel tension bars. Journal of Advanced Concrete Technology. 2018;16(11):531-548. https://doi.org/10.3151/jact.16.531